Available online at www.sciencedirect.com
ScienceDirect
Journal of Solid State Chemistry 180 (2007) 8–15
JOURNAL OF SOLID STATE CHEMISTRY
www.elsevier.com/locate/jssc

$Ag_3Ni_2O_4$—A new stage-2 intercalation compound of 2H–$AgNiO_2$ and physical properties of 2H–$AgNiO_2$ above ambient temperature

Timo Sörgel, Martin Jansen*

Max-Planck-Institut für Festkörperforschung, Heisenbergstr. 1, 70569 Stuttgart, Germany

Received 29 June 2006; received in revised form 29 August 2006; accepted 31 August 2006
Available online 23 September 2006

Abstract

$Ag_3Ni_2O_4$ was obtained as single crystals from a mixture of 2H–$AgNiO_2$ and Ag_2O in oxygen high-pressure autoclaves ($P6_3/mmc$ (no. 194), $a = 2.9331(6)$, $c = 28.313(9)$ Å, $Z = 2$). It may be regarded as a stage-2 intercalation compound of the host 2H–$AgNiO_2$ and is the first staging compound constituted of alternating subvalent $^2_\infty Ag_2^+$ and Ag^+ sheets, inserted between NiO_2^- slabs. From a structural point of view, $Ag_3Ni_2O_4$ represents an intermediate between $AgNiO_2$ and the recently reported Ag_2NiO_2. The electronic structures of 2H–$AgNiO_2$ and $Ag_3Ni_2O_4$ have been investigated based on DFT band structure calculations. The high-temperature characteristics of the starting material 2H–$AgNiO_2$ were investigated. The inverse magnetic susceptibility, electrical resistivity and differential scanning calorimetry (DSC) show a phase transition in the temperature range of $T = 320-365$ K.
© 2006 Elsevier Inc. All rights reserved.

Keywords: Layer compounds; Silver nickelates; Intercalation; Staging; Subvalency

1. Introduction

Ternary silver oxides are known to show a rich and interesting structural chemistry which is associated with extended clustering in the silver sublattice [1,2]. Since these Ag^+ substructures represent sections of the structure of elemental silver, showing the same interatomic separations, it has been suggested that silver should be susceptible to form subvalent compounds [2]. Indeed, a number of them have been realized till now, showing various structural motives and oxidation states of silver. $Ag_{13}OsO_6$ contains silver atom centered icosahedra Ag_{13}^{4+} with silver in the subvalent state of $+4/13$ [3]. A two-dimensional arrangement in the form of $^2_\infty Ag_2^+$ layers, which can again be seen as a section of elemental silver metal, was found previously in the binary fluoride Ag_2F [4]. Recently, a first ternary compound, Ag_2NiO_2, was reported to also be constituted of $^2_\infty Ag_2^+$ layers, coexisting with nickel in the oxidation state $+3$, as proven by the magnetic susceptibility, X-ray absorption near edge structure spectroscopy and quantum chemical calculations [5,6].

In this paper, we report on the synthesis of single crystals of $Ag_3Ni_2O_4$, which may be regarded as a stage-2 intercalate of 2H–$AgNiO_2$ [7].

2. Experimental

Reacting 2H–$AgNiO_2$ with Ag_2O has yielded $Ag_3Ni_2O_4$ as main product besides Ag_2NiO_2.

$Ag_3Ni_2O_4$ crystals were found in experiments with varying molar ratios, temperatures, oxygen pressures and mineralizers. Here we report on a synthesis which leads to an optimal proportion of $Ag_3Ni_2O_4$ in the product batch.

Ag_2O was precipitated from an aqueous $AgNO_3$ (p.a., Roth) solution by dropwise adding of an aqueous KOH (p.a., Roth) solution. The precipitate was washed with distilled water and dried overnight at 373 K. 2H–$AgNiO_2$ was synthesized as reported elsewhere [7]. About 396 mg of 2H–$AgNiO_2$ and 116 mg Ag_2O were thoroughly ground and transferred into a gold ampoule. About 1 mL of a 5 M KOH solution was added as a mineralizer. The ampoule was heated in an oxygen high-pressure autoclave at a rate

*Corresponding author. Fax: +49 711 689 1502.
E-mail address: m.jansen@fkf.mpg.de (M. Jansen).

0022-4596/$ - see front matter © 2006 Elsevier Inc. All rights reserved.
doi:10.1016/j.jssc.2006.08.033

of 100 K/h to 823 K where it was kept for 70 h under an oxygen pressure of 130 MPa. Then it was cooled to room temperature at a rate of −100 K/h and the products were washed with distilled water.

Powder X-ray data were recorded on a Stoe Stadi P diffractometer (*Stoe & Cie, Darmstadt, Germany*). An external standard (Si, $a = 5,43088(4)$ Å) was applied.

Single crystal X-ray data were recorded on a SMART-APEX CCD diffractometer (*Bruker AXS Inc., Madison, USA*) with graphite-monochromated Mo$K\alpha$ radiation. The reflection intensities were integrated with the SAINT [8] subprogram in the SMART [9] software package. An empirical absorption correction (SADABS [10]) was applied. The crystal structure was solved by direct methods and refined by full-matrix least squares using the SHELXTL software package [11].

Magnetic susceptibilities were determined with a Quantum Design SQUID magnetometer MPMS type 7.0 (*Quantum Design, San Diego, USA*) in the temperature range $5\,K < T < 400\,K$. A powder sample ($m \approx 120$ mg) was placed into a high-purity quartz glass tube (*Suprasil, Heraeus, Hanau, Germany*) which was subsequently evacuated and flooded with helium gas under reduced pressure. The molar susceptibility was corrected for the diamagnetic contribution of the closed shell electrons [12].

The resistivity was measured as a function of temperature employing the van der Pauw method [13]. Four Pt wires served as Ohmic electrical contacts and were pressed together with the powder (diameter: 6 mm, thickness: ≈1 mm).

Differential scanning calorimetry (DSC) measurements were performed on a DSC 404 unit (*Netzsch, Selb, Germany*) in aluminum crucibles at a heating rate of 10 K/min.

DFT calculations were performed on the basis of the experimental structures of 2H–$AgNiO_2$ [7] and $Ag_3Ni_2O_4$ (this work). The TB-LMTO-ASA program [14] (**T**ight **B**inding **L**inear **M**uffin **T**in **O**rbital calculations within the **A**tomic **S**phere **A**pproximation) was used choosing the scalar relativistic option and the **L**ocal **D**ensity **A**pproximation (LDA) functional of v. Barth and Hedin [15] to describe the exchange and correlation interaction. The radii of the atomic spheres and additional empty spheres to minimize the overlap of the atomic spheres [16] were determined by applying the standard procedures of the program. Due to the downfolding process, for oxygen only the 2p states were considered in the starting configuration of the calculation.

The Hartree–Fock calculations were performed with the program Crystal [17] and the basis sets and pseudo potentials were taken from the work of Wedig et al. [18].

Table 1
Experimental details on the X-ray single crystal investigation of $Ag_3Ni_2O_4$

Formula weight (g/mol)	504.99
Temperature (K)	298(2)
Wave length (Å)	0.71073
Crystal size (mm^3)	0.15 · 0.15 · 0.10
Crystal system; space group (no.)	Hexagonal; $P6_3/mmc$ (194)
Lattice parameters (Å)	$a = 2.9331(6)$ $c = 28.313(9)$
Volume (Å^3); Z	210.94(9); 2
$\rho_{X\text{-ray}}$ (g/cm^3), μ (mm^{-1})	7.951; 22.328
Diffractometer	Bruker AXS Smart APEX, Mo$K\alpha$ radiation, graphite monochromator, ω-scans
2θ range (°)	1.44–34.91
hkl range	$-4 \leqslant h \leqslant 4$, $-4 \leqslant k \leqslant 4$, $-44 \leqslant l \leqslant 44$
No. of measured reflections; R_{int}	2800; (R(int) = 0.0298)
No. of independent reflections	237
Completeness to theta = 34.91°	92.5%
Absorption correction	Multiscan[a]
Data/restraints/parameters	237/0/16
Goodness-of-fit on F^2	1.353
Final R-values ($I > 2\sigma(I)$)	$R_1 = 5.17\%$, w$R_2 = 10.41\%$
R-values (all data)	$R_1 = 5.60\%$, w$R_2 = 11.74\%$
ΔF_{max}; ΔF_{min} (e/Å^3)	3.560; −3.811

[a]SADABS: V. 2.10 G. M. Sheldrick, Bruker AXS Inc., Madison, USA (2003).

Table 2
Atomic coordinates and equivalent isotropic displacement parameters (in Å^2) for $Ag_3Ni_2O_4$

Atom	Position	x	y	z	U(eq)
Ag1	2c	1/3	2/3	1/4	0.013(1)
Ag2	4f	1/3	2/3	0.0402(1)	0.016(1)
Ni1	4f	1/3	2/3	0.8580(1)	0.011(1)
O1	4f	1/3	2/3	0.1774(5)	0.015(3)
O2	4e	0	0	0.8949(5)	0.015(3)

U(eq) is defined as one third of the trace of the orthogonalized U_{ij} tensor.

Table 3
Anisotropic displacement parameters (in Å^2) for $Ag_3Ni_2O_4$, in the form $\exp(-2\pi^2(h^2a^{*2}U_{11} + \ldots + 2hka^*b^*U_{12}))$

Atom	U_{11}	U_{22}	U_{33}	U_{23}	U_{13}	U_{12}
Ag1	0.014(1)	0.014(1)	0.011(1)	0	0	0.007(1)
Ag2	0.017(1)	0.017(1)	0.013(1)	0	0	0.009(1)
Ni1	0.011(1)	0.011(1)	0.012(1)	0	0	0.005(1)
O1	0.018(4)	0.018(4)	0.011(5)	0	0	0.009(2)
O2	0.014(4)	0.014(4)	0.018(6)	0	0	0.007(2)

3. Results

According to a single crystal structure analysis, $Ag_3Ni_2O_4$ is hexagonal ($P6_3/mmc$). Experimental crystal structure details and selected bond lengths and angles are given in Tables 1–4 [19].

In the product mixture, which was investigated by X-ray powder diffraction, $Ag_3Ni_2O_4$, 2H–$AgNiO_2$ and Ag_2NiO_2

Table 4
Selected bond lengths and angles for $Ag_3Ni_2O_4$

Connected atoms	Distance/angle (Å/°)
Ag1–O1 (2*x*)	2.06(1)
Ag2–O2 (3*x*)	2.50(1)
Ag1–Ag1 (6*x*)	2.9331(6)
Ag2–Ag2 (3*x*)	2.837(2)
Ag2–Ag2 (6*x*)	2.9331(6)
Ni1–O1 (3*x*)	1.967(6)
Ni1–O2 (3*x*)	1.990(8)
Ni1–Ni1 (6*x*)	2.9331(6)
O1–Ag1–O1 (1*x*)	180.0
O1–Ni1–O(1) (3*x*)	96.4(5)
O1–Ni1–O(2) (6*x*)	84.3(4)
O1–Ni1–O(2) (3*x*)	178.9(5)
O2–Ni1–O(2) (3*x*)	95.0(5)
Ni1–O1–Ni1 (3*x*)	96.4(5)
Ni1–O2–Ni1 (3*x*)	95.0(5)
Ni1–O1–Ag1 (3*x*)	120.6(4)
Ni1–O2–Ag2 (6*x*)	95.6(2)
Ni1–O2–Ag2 (3*x*)	164.3(6)
Ag2–O2–Ag2 (3*x*)	71.9(4)
Ag2–Ag2–Ag2 (3*x*)	58.87(3)
Ag2–Ag2–Ag2 (6*x*)	60.0
Ag2–Ag2–Ag2 (3*x*)	62.26(6)
Ag2–Ag2–Ag2 (6*x*)	90.0
Ag2–Ag2–Ag2 (6*x*)	120.0
Ag2–Ag2–Ag2 (6*x*)	121.13(3)
Ag2–Ag2–Ag2 (3*x*)	180.0

were found. Additional weak Bragg reflections could be indexed with a unit cell, corresponding to the metrics of a potential 2H–Ag_2NiO_2 ($a = b = 8,798(5)$ and $c = 16,135(5)$ Å, corresponding to $a = 3a(3R–Ag_2NiO_2)$ and $c = (2/3)c(3R–Ag_2NiO_2)$).

The dominating structural feature of $Ag_3Ni_2O_4$ is NiO_2^- layers which are stacked along the *c*-axis alternating with Ag^+-single and Ag_2^+-double layers (Fig. 1). Thus the new oxide can be written as $Ag^{+1}Ag_2^{+0.5}Ni_2^{+3}O_4^{-2}$, or $Ag^{+1}Ni^{+3}O_2^{-2} \cdot Ag_2^{+0.5}Ni^{+3}O_2^{-2}$, respectively. It is an intermediate between $AgNiO_2$ and Ag_2NiO_2, yet the polytype is of 2H instead of 3R type [20]. This intermediate character is supported by the bond distances and angles, which are close to those in 2H–$AgNiO_2$ and Ag_2NiO_2. The bond distances in the Ag1-single layers are slightly shortened as compared to 2H–$AgNiO_2$ (0.1%), while they are elongated by 0.3% and 0.5%, respectively, in the Ag2-double layers as compared to Ag_2NiO_2. As the silver single and double layers are commensurate, the Ag1–Ag1 and Ag2–Ag2 distances in the *a*–*b*-plane are all equal and amount to 2.9331(6) Å. The distance between the Ag_2^+ layers in $Ag_3Ni_2O_4$ is in the nanometer range ($c/2 = 14.16$ Å), in contrast to the respective distance in Ag_2NiO_2 ($c/3 = 8.03$ Å).

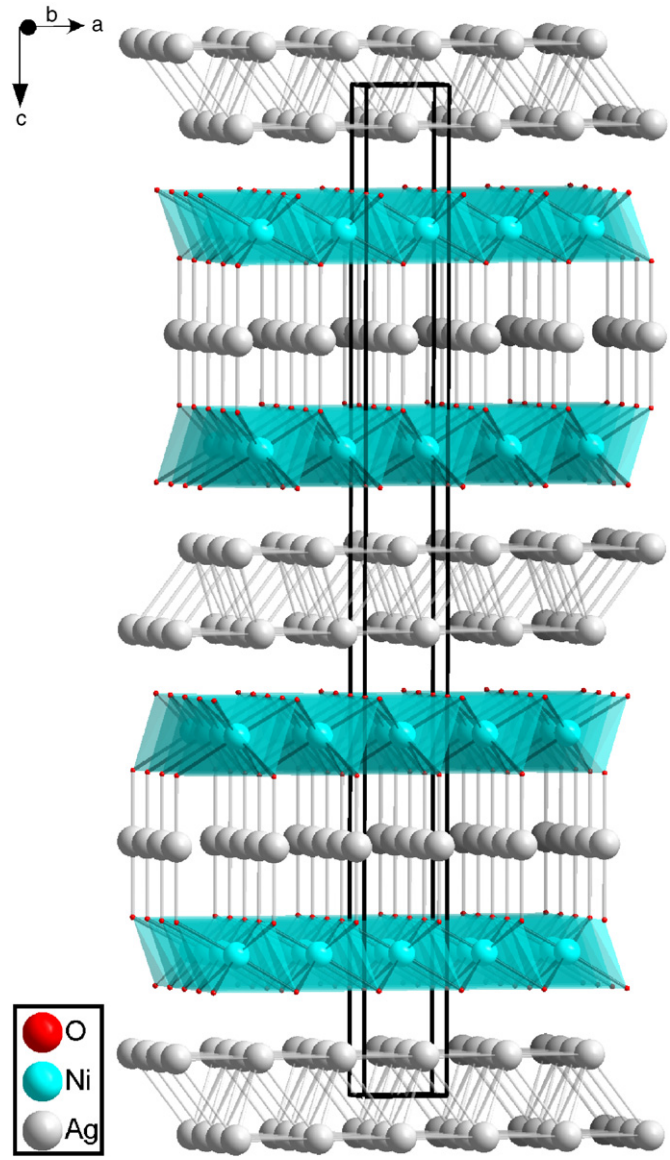

Fig. 1. Structure of $Ag_3Ni_2O_4$ with unit cell.

The NiO_2^- layers in $Ag_3Ni_2O_4$ differ from those in 2H–$AgNiO_2$ [7] and Ag_2NiO_2 [5] (at $T > 260$ K), as the Ni–O distances are no longer equal. This is due to the different coordinations of the oxide ions, which are tetrahedral ($O1Ni_3Ag1$) and octahedral ($O2Ni_3Ag2_3$), respectively. However, also in $Ag_3Ni_2O_4$ there is obviously a spin-1/2 triangular lattice like in $AgNiO_2$ and Ag_2NiO_2, which is responsible for a variety of phase transitions driven by orbital and spin ordering in these compounds.

Ag_2NiO_2 undergoes a Jahn–Teller phase transition at $T_S = 260$ K [18], while for 2H–$AgNiO_2$ no structural phase transition was noticed in the investigated range 5–400 K [21,22]. Instead, an electronically driven phase transition occurs in the range of $T = 320–365$ K, which can be derived from susceptibility and electrical resistivity measurements. The inverse magnetic susceptibility of 2H–$AgNiO_2$ (Fig. 2) reveals, apart from the antiferromagnetic phase transition at $T = 22$ K which has been

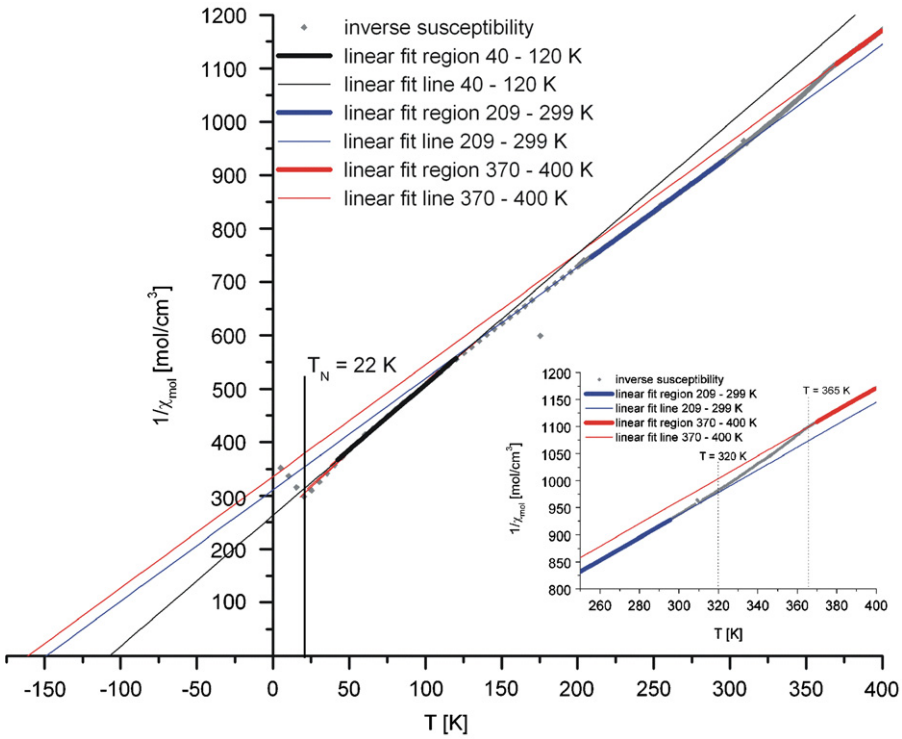

Fig. 2. Inverse magnetic susceptibility of 2H–$AgNiO_2$ up to $T = 400$ K.

discussed elsewhere [7,21,22], two Curie–Weiss regions in the range of 22 K $< T <$ 320 K. The data points were fitted independently for the intervals 40–120 and 209–299 K. This has led to magnetic moments of $\mu_{eff} = 1.81\,\mu_B$, and $1.96\,\mu_B$, and Weiss constants of $\Theta_P = -107$, and -149 K, respectively. In the range of 320 K $< T <$ 365 K, there is a smooth step into a third high-temperature Curie–Weiss region, with $\mu_{eff} = 1.96\,\mu_B$ and $\Theta_P = -161$ K (fit of data points in the range 370–400 K).

The resistivity measurement above room temperature shows a step-like decrease between two metallic regimes in the range 325 K $< T <$ 365 K. The conductivity improves by about 5%.

Fig. 3 shows the resistivity normalized to ρ(310 K), which shows a decrease of the resistivity by 5% upon the phase transition. The resistivity below room temperature was published elsewhere [7].

DSC measurements show a reversible phase transition with small peaks at $T = 358$ K (heating experiment) and $T = 354$ K (cooling experiment).

The band structures were calculated for 2H–$AgNiO_2$ and $Ag_3Ni_2O_4$ on DFT basis. They were performed without spin polarization, as spin polarized calculations did not converge. As is known for spin polarized calculations which were performed for 3R–$AgNiO_2$ and Ag_2NiO_2 on a mixed Hartree–Fock and DFT basis, the results are very similar to the ones obtained from non-spin polarized calculations with respect to band structure characteristics and density of states (DOS) [18]. Therefore it was concluded that in the family of silver nickelates, non-spin polarized calculations are sufficient to deduce the essential features of the band structures.

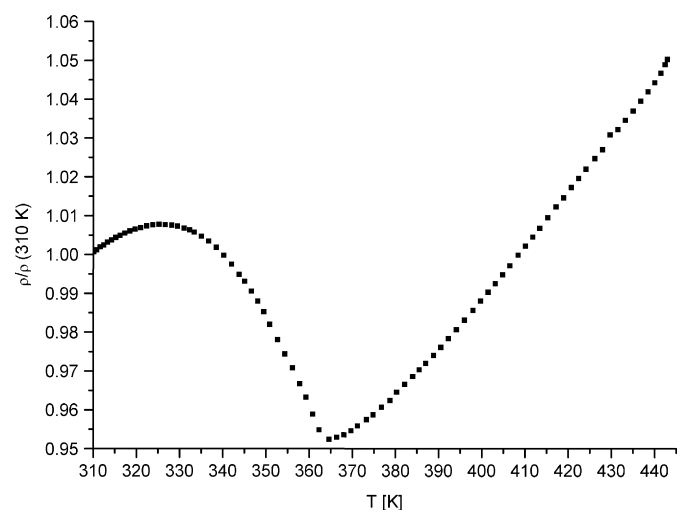

Fig. 3. Resistivity ρ of 2H–$AgNiO_2$, relative to ρ(310 K).

The band structure of 2H–$AgNiO_2$ in the fatband presentation is shown for Ag-4p, Ag-5s and -5p, Ni-3d and O-2p states in Fig. 4. Ni-3d and O-2p states dominate at the Fermi level, which can be seen from the partial DOS in Fig. 5. Yet, also Ag-5s, -5p and -4d states contribute to the highest occupied bands. The integrated partial DOS (IDOS) shows that the Ag-4d states are not fully occupied and more than half an electron is promoted into Ag-5s and -5p states (Table 5). In contrast to the band structure of

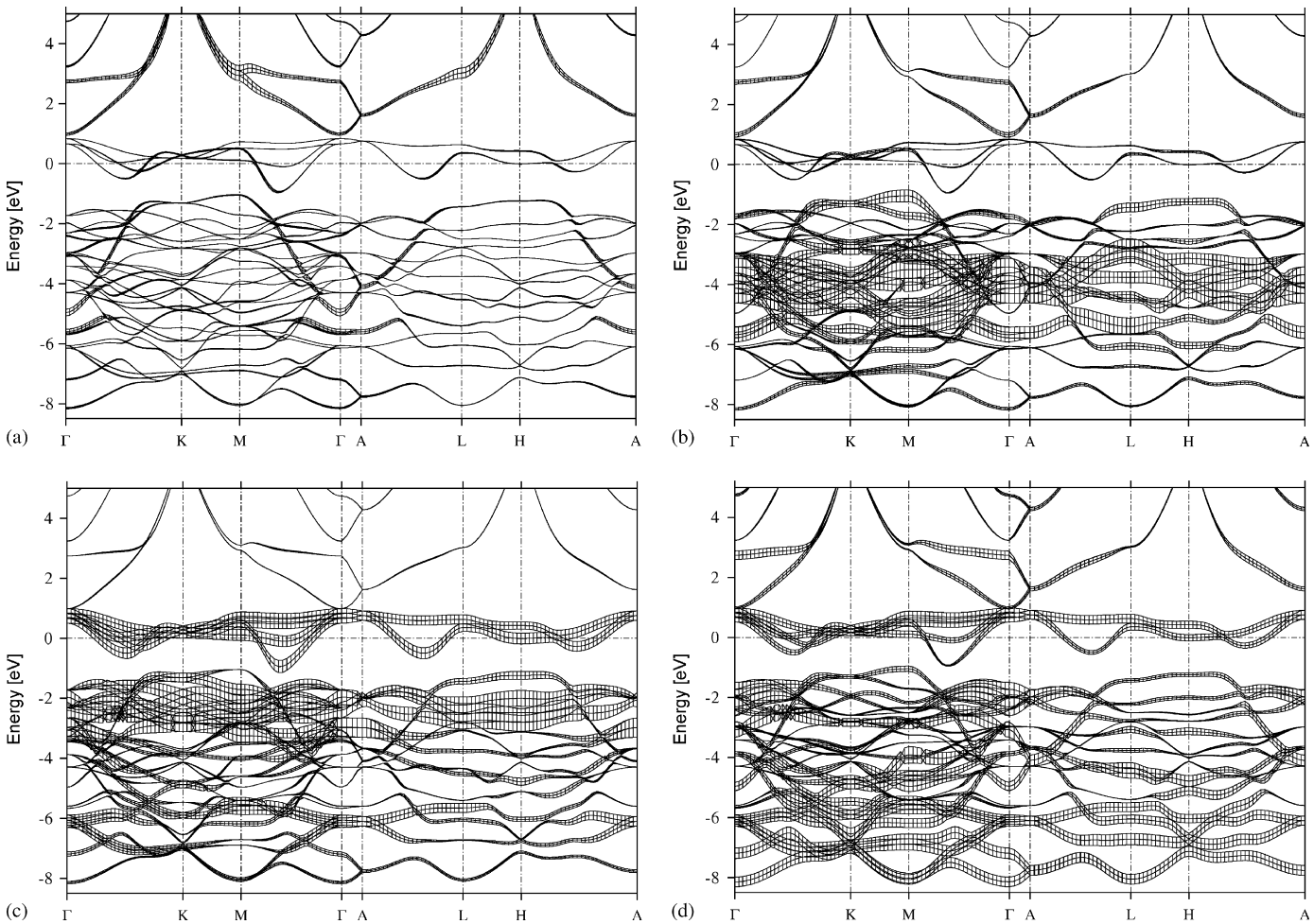

Fig. 4. Band structure of 2H–$AgNiO_2$ with fatbands of (a) Ag-5s and -5p, (b) Ag-4d, (c) Ni-3d and (d) O-2p states.

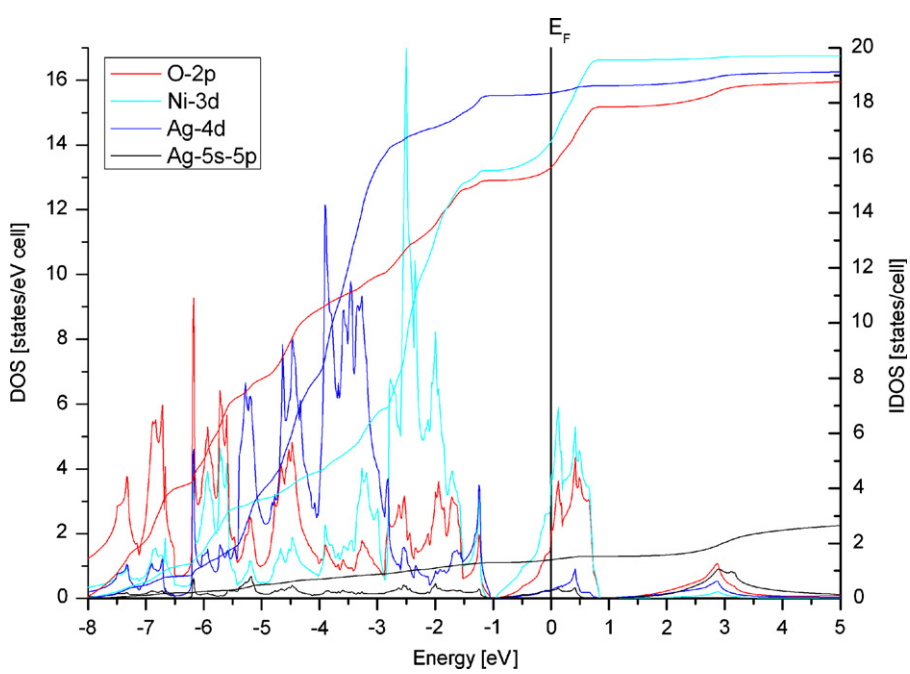

Fig. 5. Partial DOS and IDOS of the Ag-5s and -5p, Ni-3d and O-2p states in 2H–$AgNiO_2$.

3R-$AgNiO_2$ [21,23], Ag-4d states occupy bands very close to the Fermi level.

For $Ag_3Ni_2O_4$ the band structure is also shown in fatband representation for the Ag-5s and -5p, Ag-4d (Fig. 6), Ni-3d and O-2p states (Fig. 7). The band structure is more complex than the one of 2H–$AgNiO_2$, and it shows the characteristics of both the band structures of 2H–$AgNiO_2$ and Ag_2NiO_2 [21]. The 5s and 5p states of Ag2, which make up the Ag_2^+ layers, contribute more pronouncedly to the states at the Fermi level than those of Ag1, which constitutes the single Ag^+ layers (see DOS in Fig. 8). Yet, the states of Ni-3d and O-2p still dominate the Fermi level. Like in 2H–$AgNiO_2$, the Ag1-4d states contribute to bands right below the Fermi level, whereas the Ag2-4d states correspond more to the Ag-4d states found in Ag_2NiO_2 and contribute to bands of lower energies. From the partial IDOS, it is evident that Ag2 is subvalent in contrast to Ag1, as there is more than one electron in addition in Ag2 states (see Table 6).

Table 5
Integrated DOS for Ag, Ni, O, E and E1 in 2H–$AgNiO_2$ (E and E1 = empty spheres)

Atom	IDOS(s) (states/cell)	IDOS(p) (states/cell)	IDOS(d) (states/cell)
Ag	0.41	0.29	9.18
Ni	0.39	0.54	8.30
O	0.07	3.91	0.06
E	0.25	0.25	0.12
E1	0.16	0.09	—

4. Discussion

In 2H–$AgNiO_2$, the changes in the course of the inverse magnetic susceptibility and the electrical resistivity at $T > 320$ K might be due to spin and orbital ordering. There are a number of degenerate states so that a change in the ordering pattern may easily occur upon temperature change. The range of the transition between the second and third Curie–Weiss region corresponds well with the temperature region where $d\rho/dT$ is negative. In 3R–$AgNiO_2$, a negative slope in $d\rho/dT$ is reported for $T > 300$ K [24], yet there is no report on a change into a further region with $d\rho/dT > 0$ at higher temperatures.

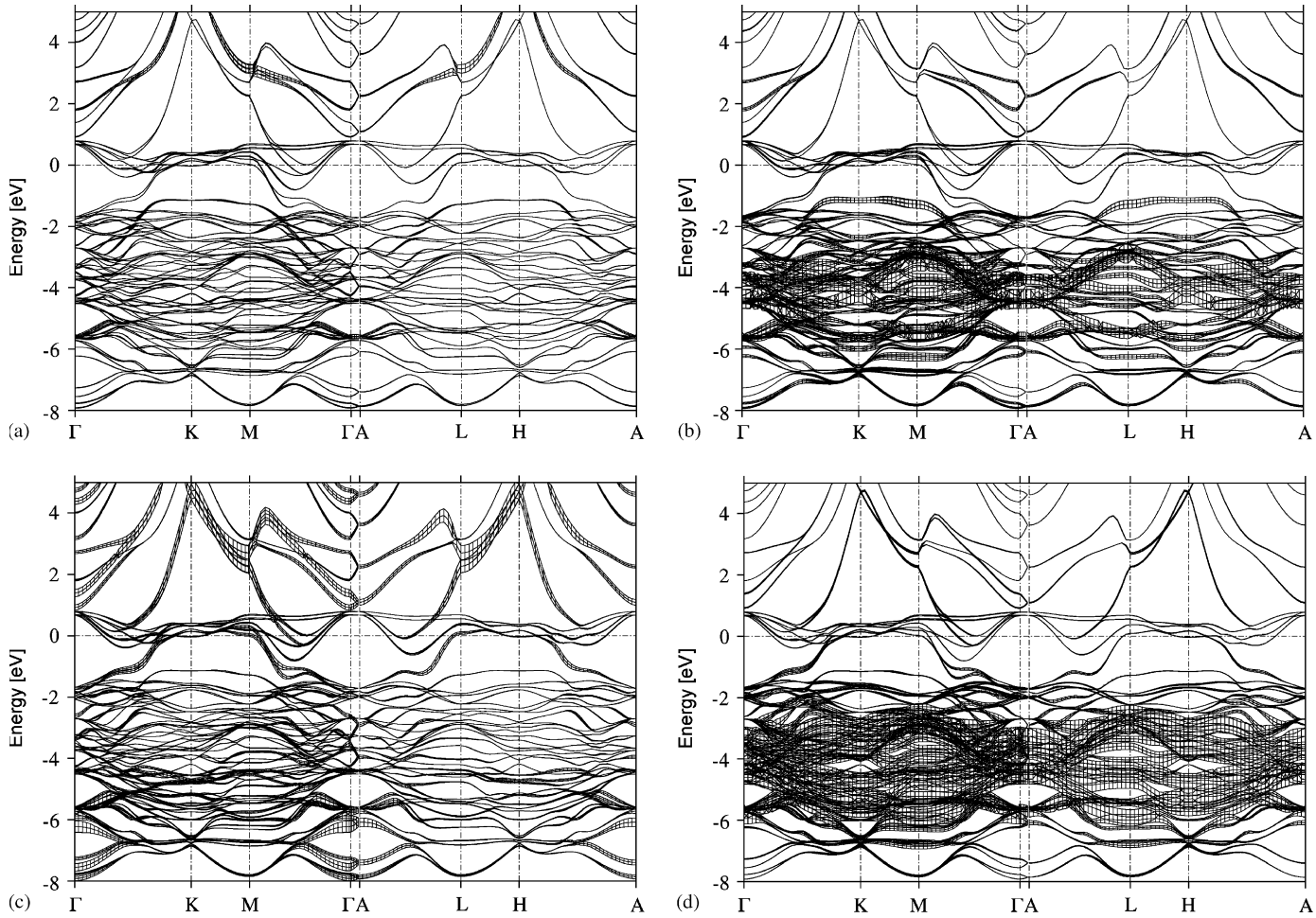

Fig. 6. Band structure of $Ag_3Ni_2O_4$ with fatbands for (a) Ag1-5s and -5p, (b) Ag1-4d, (c) Ag2-5s and -5p and (d) Ag2-4d states.

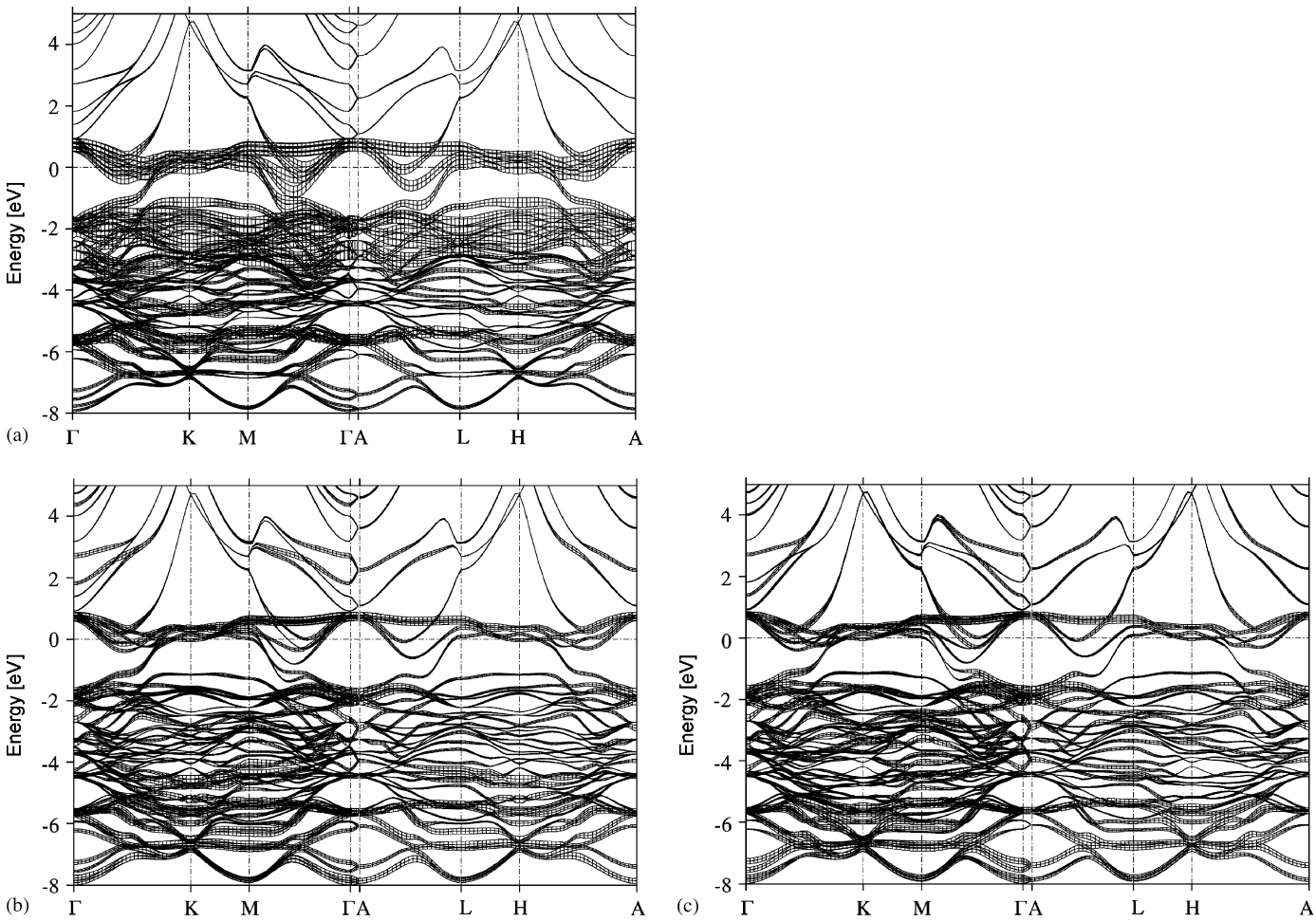

Fig. 7. Band structure of $Ag_3Ni_2O_4$ with fatbands for (a) Ni-3d, (b) O1-2p and (c) O2-2p states.

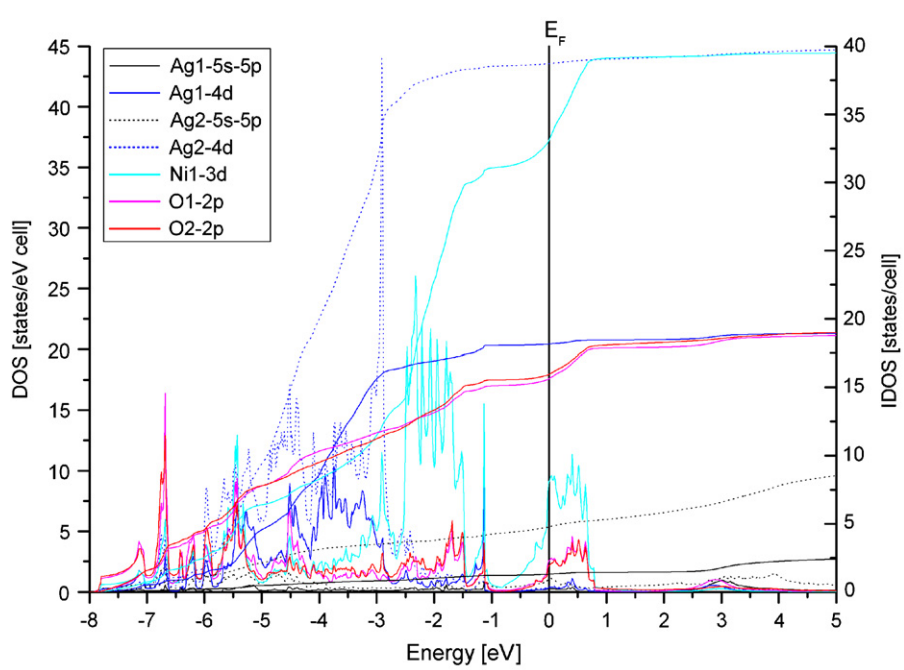

Fig. 8. Partial DOS and IDOS of the Ag1-5s and -5p, Ag1-4d, Ag2-5s and -5p, Ag2-4d, Ni1-3d, O1-2p and O2-2p states in $Ag_3Ni_2O_4$.

Table 6
Integrated DOS for Ag1, Ag2, Ni1, O1, O2, E, E1 and E2 in $Ag_3Ni_2O_4$ (E, E1 and E2 = empty spheres)

Atom	IDOS(s) (states/cell)	IDOS(p) (states/cell)	IDOS(d) (states/cell)
Ag1	0.39	0.26	9.08
Ag2	0.62	0.58	9.68
Ni1	0.37	0.52	8.28
O1	0.07	3.91	0.06
O2	0.09	3.99	0.05
E	0.26	0.26	0.13
E1	0.17	0.10	—
E2	0.19	0.15	—

Since $Ag_3Ni_2O_4$ is only obtained if 2H–$AgNiO_2$ is used as an educt, of which the stacking sequence of Ni- and O-layers only slightly differs from the one in $Ag_3Ni_2O_4$, we suggest that $Ag_3Ni_2O_4$ forms in a topotactic-like reaction. The sum of activation energies for this intercalation process is lower, since apart from widening of the structure, less rearrangement of the Ni- and O layers is needed as compared to 3R–$AgNiO_2$.

The observations can also be rationalized in terms of thermodynamics. The free enthalpy ΔG of the reaction is likely to be less negative upon staging, as compared to a total intercalation process. ΔG of the reaction 3R–$AgNiO_2 + Ag \rightarrow Ag_2NiO_2$ was estimated from open cell voltage measurements to be ≈ -5 kJ/mol at $T = 500$ K [21]. Upon staging, the system reduces its free enthalpy by a smaller extent. Assuming an intercalation of 3R–$AgNiO_2$, upon which a hypothetical stage-3 compound is formed, this would be one third, which might explain why such a stage-3 phase was not observed, so far. For the intercalation of 2H–$AgNiO_2$, this is approximately one half. From open cell voltage measurements on a cell 2H–$AgNiO_2$/AgI/Ag, the free enthalpy was derived as $\Delta G \approx -2.5$ kJ/mol [21].

To summarize, it can be concluded that silver nickelates might be accessible in a variety of compositions, which are all very close regarding their free enthalpies of formation. It is possible that, due to different activation energies, the reaction paths chosen still depend on the structural details of the starting material. Due to their structural similarity, $Ag_3Ni_2O_4$ was only obtained when starting from 2H–$AgNiO_2$, whereas Ag_2NiO_2 is the only product when starting from 3R–$AgNiO_2$.

$Ag_3Ni_2O_4$ contains spin-1/2 Ni^{3+} ions on a triangular lattice, yet due to the different environment of the NiO_2^- sheets, Ni^{3+} finds itself, unlike as in $AgNiO_2$ and Ag_2NiO_2, in a distorted coordination with oxygen. This may lead again to a different physical behavior. Concerning the silver sublattice, $Ag_3Ni_2O_4$ is an intermediate between $AgNiO_2$ and Ag_2NiO_2, showing Ag(I) and subvalent Ag(+0.5) in one single compound.

Acknowledgments

We thank Dr. U. Wedig for the Hartree–Fock calculation and discussion, Dr. J. Nuss for the single crystal X-ray data collection, E. Brücher for the magnetic susceptibility measurement and G. Siegle for the electrical resistivity measurement.

References

[1] M. Jansen, J. Less-Common Met. 76 (1980) 285.
[2] M. Jansen, Angew. Chem. 99 (1987) 1136;
M. Jansen, Angew. Chem. Int. Ed. Engl. 26 (1987) 1098.
[3] S. Ahlert, W. Klein, O. Jepsen, O. Gunnarsson, O.K. Andersen, M. Jansen, Angew. Chem. 115 (2003) 4458;
S. Ahlert, W. Klein, O. Jepsen, O. Gunnarsson, O.K. Andersen, M. Jansen, Angew. Chem. Int. Ed. Engl. 42 (2003) 4322.
[4] G. Argay, F. Naray-Szabo, Acta Chim. Acad. Sci. Hung. 239 (1966).
[5] M. Schreyer, M. Jansen, Angew. Chem. 114 (2002) 665;
M. Schreyer, M. Jansen, Angew. Chem. Int. Ed. Engl. 41 (2002) 643.
[6] H. Yoshida, Y. Muraoka, T. Sörgel, M. Jansen, Z. Hiroi, Phys. Rev. B 73 (2006) 020408(R).
[7] T. Sörgel, M. Jansen, Z. Anorg. Allg. Chem. 631 (2005) 2970.
[8] SAINT Version 6.45, Bruker AXS Inc., Madison, USA, 2003.
[9] SMART Version 5.630, Bruker AXS Inc., Madison, USA, 1997.
[10] G.M. Sheldrick, SADABS 2.10, Bruker AXS Inc., Madison, USA, 2001.
[11] G.M. Sheldrick, SHELXTL 6.12, Bruker AXS Inc., Madison, USA, 2000.
[12] A. Weiss, H. Witte, Magnetochemie, Verlag Chemie, Weinheim, 1973.
[13] L.J. Van der Pauw, Philips Res. Rep. 13 (1958) 1.
[14] O.K. Andersen, O. Jepsen, Tight Binding Linearized Muffin Tin Orbital Method Within the Atomic Sphere Approximation, Version 4.7, Stuttgart, Germany, 1996.
[15] U. Von Barth, L. Hedin, J. Phys. C 5 (1972) 1629.
[16] O.K. Andersen, A.V. Postnikov, S.Y. Savrasov, The muffin-tin orbital point of view, in: W.H. Butler, P.H. Dederichs, A. Gonis, R.L. Weaver (Eds.), Applications of Multiple Scattering Theory to Materials Science, vol. 253, Materials Research Symposium Proceedings, Pittsburgh, 1992, pp. 37–70.
[17] V.R. Saunders, R. Dovesi, C. Roetti, M. Causa, N.M. Harrison, R. Orlando, C.M. Zicovich-Wilson, CRYSTAL98, CRYSTAL98 User's Manual, University of Torino, Torino, 1998.
[18] U. Wedig, P. Adler, J. Nuss, H. Modrow, M. Jansen, Solid State Sci. 8 (2006) 753.
[19] Further details of the crystal structure investigation can be obtained from the Fachinformationszentrum Karlsruhe, 76344 Eggenstein-Leopoldshafen, Germany (fax: (49) 7247-808-666; e-mail: crysdata@fiz-karlsruhe.de) on quoting the depository number CSD-416735.
[20] L.S. Ramsdell, Am. Miner. 32 (1947) 64.
[21] T. Sörgel, Dissertation, University of Stuttgart, 2006; The Publication Server of the University of Stuttgart, available through 〈http://elib.uni-stuttgart.de/opus/〉, to be published.
[22] E. Wawrzynska, E. M. Wheeler, R. Coldea, T. Sörgel, M. Jansen, in preparation.
[23] R. Seshadri, C. Felser, K. Thieme, W. Tremel, Chem. Mater. 10 (1998) 2189.
[24] Y.J. Shin, J.P. Doumerc, P. Dordor, C. Delmas, M. Pouchard, P. Hagenmuller, J. Solid State Chem. 107 (1993) 303.